Double-PI Speed Control with Anti-Windup for a PMSM Drive with Hysteresis Current Controller

Md Hairul Nizam Talib [1*], Jurifa Mat Lazi [1], Azrita Alias [1], Fazlli Patkar [1], Nurul Ain Said [1], Zainuddin Mat Isa [2]

[1] Fakulti Teknologi dan Kejuruteraan Elektrik, Universiti Teknikal Malaysia Melaka, Melaka, Malaysia.

[2] Fakulti Kejuruteraan dan Teknologi Elektrik, Universiti Malaysia Perlis, Perlis, Malaysia.

DOI: https://doi.org/10.47772/IJRISS.2026.101000133

Received: 11 October 2026; Accepted: 16 October 2026; Published: 30 October 2026

ABSTRACT

Permanent magnet synchronous motor (PMSM) drives require accurate speed regulation under changing operating conditions. In a conventional proportional-integral (PI) speed controller, saturation of the torque-producing current command can cause integrator windup and degrade the transient response. This study evaluates a double-PI controller with anti-windup compensation (DAWPI) for a field-oriented PMSM drive employing hysteresis current control. A MATLAB/Simulink model is used to compare conventional PI, anti-windup PI (AWPI), and DAWPI controllers during start-up, load application, and operation at different reference speeds. The modeled drive includes the electrical and mechanical PMSM dynamics, coordinate transformations, a two-level voltage-source inverter, hysteresis current regulation, and an outer speed-control loop. The comparison considers speed overshoot, rise time, settling time, steady-state error, and transient torque and phase-current responses. No-load tests examine the responses at rated, medium, and low reference speeds, while the load test examines speed deviations during load application and removal. At a reference speed of 1500 rpm, the speed overshoots are 17.93%, 3.07%, and 1.60% for PI, AWPI, and DAWPI, respectively. These results indicate that DAWPI further suppresses rated-speed overshoot relative to AWPI in the evaluated operating case. The study provides a simulation-based comparison of the three controller configurations and considers the trade-off between transient speed deviations and recovery behavior. The reported overshoot comparison does not by itself establish an improvement in every performance measure. Conclusions about robustness, implementation cost, and practical operation require supporting quantitative results or experimental validation. Future experimental implementation can assess the influence of switching delays, measurement noise, and hardware limitations on the simulated performance.

Keywords: PMSM, field-oriented control, hysteresis current control, double-PI speed controller, anti-windup

INTRODUCTION

Permanent magnet synchronous motors (PMSMs) are attractive for variable-speed drives because of their high efficiency, power density, and compact construction [5], [8]. Accurate torque and speed regulation remains important when the reference or mechanical load changes, motivating evaluation of the speed controller and its interaction with current regulation. Wang and Leng reviewed the development of PMSMs [15], while Saidur et al. discussed the role of variable-speed drives in adapting motor operation to application demand and identifying energy-saving opportunities [10].

Field-oriented control (FOC) expresses the stator-current vector in a reference frame aligned with the rotor magnetic field. Direct- and quadrature-axis components permit separate treatment of flux-related and torque-producing current demands. The outer speed controller generates the torque-producing current reference, while the inner stage regulates the motor currents [8], [9]. PMSM modeling, control methods, and rotor-position estimation are also addressed in the monograph by Wang et al. [14].

Voltage-source inverter modulation provides another means of implementing FOC. Wang et al. investigated a simulated PMSM drive using space-vector pulse-width modulation (SVPWM) [16], and Khalid et al. compared sinusoidal PWM and SVPWM in a vector-controlled PMSM drive [6]. These studies provide context for voltage-modulated implementations, whereas the present drive uses direct phase-current regulation through HCC. The same HCC configuration is retained when comparing the three speed controllers.

Hysteresis current control (HCC) changes inverter switching states when the phase-current error reaches a prescribed band boundary. This direct logic provides simple implementation and rapid current tracking without separate PI phase-current regulators [8], [9]. Fixed-band HCC has a variable switching frequency; a narrower band generally improves tracking but increases switching activity. Induction-motor experiments showed that band width substantially affects stator-current quality even when speed-response changes are small [13]. A common HCC configuration should therefore be maintained when comparing speed controllers.

PMSM applications of HCC-based FOC have been studied by Ogbuka et al., who investigated current and torque tracking together with speed responses to step and ramp commands [8], [9]. More recently, Santhakumar et al. combined HCC-FOC with an extended Clarke transformation for a five-phase PMSM supplied by a three-level inverter [11]. That work addresses a different machine and inverter topology from the present three-phase drive, but illustrates continued interest in improving the interaction between coordinate transformation and current regulation. These studies motivate evaluation of the outer speed controller within an established HCC-based drive structure.

Conventional PI control remains practical because of its simple structure and straightforward implementation. Integral action can remove steady-state speed error when the commanded action can be realized. Alternative PMSM speed-control strategies have also been investigated. Choi et al. implemented an adaptive speed regulator and evaluated its response to motor-parameter and load-torque variations [1]. Jung et al. developed online adaptive PID gain adjustment for parameter uncertainties [5]. Elmas and Ustun combined sliding-mode and neuro-fuzzy control, selecting transient and steady-state actions through an error-band mechanism [3]. These approaches motivate examining the performance achievable with a PI-based structure.

A central limitation of PI speed regulation is integrator windup when the torque or current command is saturated. The integral state can continue accumulating speed error even though the drive cannot apply the requested command. When saturation ends, the accumulated state may sustain an excessive command, increasing overshoot and delaying recovery. Choi and Lee examined this problem in a PMSM drive and proposed an anti-windup strategy that assigns an appropriate integral-state value during the transition from proportional to PI control [2]. Li et al. compared anti-windup PI strategies using a PI-plane representation and emphasized the influence of the integral state at re-entry into the unsaturated region on overshoot and settling time [7].

Anti-windup compensation therefore needs to be assessed across the relevant operating range rather than assumed to improve every response equally. In an experimental indirect-FOC induction-motor study, Talib et al. found that AWPI produced its clearest overshoot and settling-time improvements at medium and rated speeds, whereas PI and AWPI responses were similar at low speed. The compared schemes also had similar load-disturbance rejection in the reported tests [12]. Although these results concern an induction motor, they support evaluating saturation handling under several speed and load conditions and reporting both benefits and trade-offs.

Double-PI and parallel-PI structures have likewise been investigated in FOC drives. Zellouma et al. compared parallel proportional-integral control with conventional PI control in a simulated induction-motor drive, considering dynamic response, ripple, and parameter variations [17]. Hazratgholi Zadeh Namin et al. subsequently developed modified double-PI control for three-phase induction motors and operation under an open-phase fault, with experimental validation [4]. These contributions establish relevant prior work, but their findings do not determine the performance of an anti-windup double-PI speed controller in the PMSM configuration considered here.

The DAWPI configuration considered here comprises two parallel PI paths driven by the speed error. Their outputs are summed and passed through a common limiter to generate the quadrature-axis current reference. A comparison between the command before and after saturation controls a switch that selects either the speed error or zero at the first integral-path input. This arrangement is intended to inhibit integration in that path during saturation. The second integral path is continuously connected to the speed error in the supplied diagram, so its saturation behavior must be explicitly addressed when interpreting the complete controller.

Accordingly, this study evaluates conventional PI, AWPI, and DAWPI speed-control strategies in a MATLAB/Simulink model of a three-phase FOC PMSM drive with HCC. The comparison covers start-up, load application, and different reference speeds, with attention to speed overshoot, rise time, settling time, steady-state error, and transient torque and phase-current responses. The objective is to determine whether the DAWPI configuration offers an additional benefit over AWPI while identifying any response-time or transient-current trade-offs. The contribution is framed as an application-specific comparative assessment; the controller topology, anti-windup implementation, tuning procedure, and common test conditions must be stated explicitly to support reproducibility and interpretation.

METHODOLOGY

Field-oriented control and current regulation

Figure 1 shows the control structure of the FOC PSMM drive fed by hysteresis current controller. Reference and measured rotor speeds are compared to produce the speed error. The speed controller generates the torque-producing current command i_q^*, while i_d^* is set to zero for operation below to provides maximum torque per ampere applies to a surface-mounted PMSM below base speed. The inverse Park and Clarke transformation converts the d-q references into three-phase reference currents demands. Each reference is compared with its measured phase current, and the hysteresis current controllers generate the inverter switching commands and DC-link voltage supply to the PMSM.

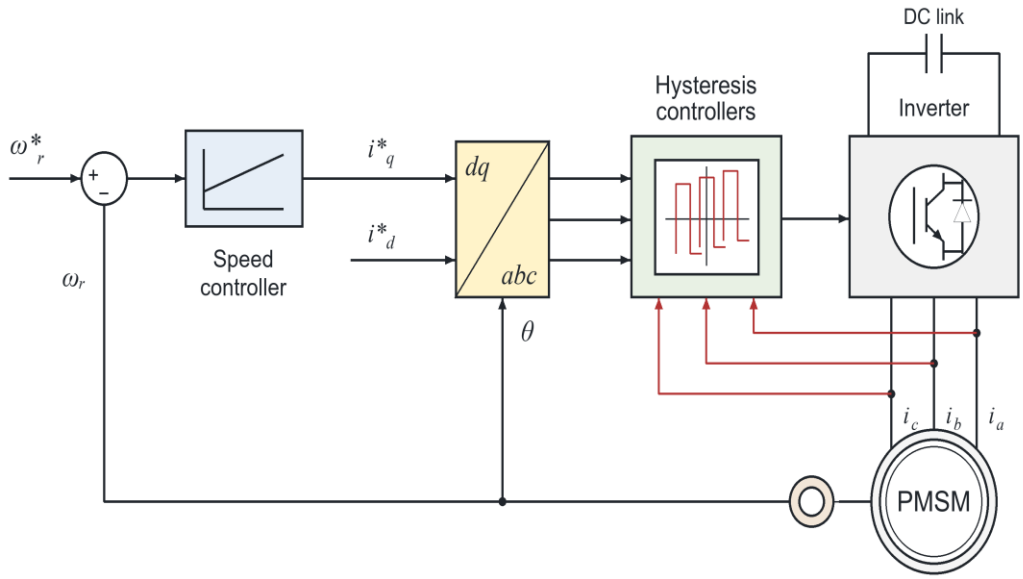

Figure 1: Control structure of the FOC-based PMSM drive using hysteresis current regulation.

Field oriented control is used to decouple the stator current of the PMSM into equivalent flux and torque producing current components for independent and precise control of torque and flux. Park and Clark Transformation are used to facilitate the variables from time varying coefficients to a common reference frame. Clarke transformation is used to change from three phase stationary frame (abc) into two phase arbitrary

stationary reference frame (αβ) where β-axis lag α-axis by 90°. The Park equation is used to convert rotating d-q frame to stationary α-β frame and vise versa. Equation 1 show the Inverse part transformation matrix:

$$\begin{matrix} I_\alpha \\ I_\beta \end{matrix} = \begin{bmatrix} \cos\theta_f & -\sin\theta_f \\ \sin\theta_f & \cos\theta_f \end{bmatrix} \begin{matrix} I_d \\ I_q \end{matrix} \quad (1)$$

Meanwhile, the reverse transformation from stationary αβ frame to three phase stationary frame (Inverse Clark Transformation) is given in equation 2.

$$\begin{bmatrix} I_a \\ I_b \\ I_c \end{bmatrix} = \begin{bmatrix} 1 & 0 \\ -\frac{1}{2} & \frac{\sqrt{3}}{2} \\ -\frac{1}{2} & -\frac{\sqrt{3}}{2} \end{bmatrix} \begin{bmatrix} I_\alpha \\ I_\beta \end{bmatrix} \quad (2)$$

PMSM mathematical model

Assuming balanced sinusoidal operation, negligible magnetic saturation, and a synchronously rotating d-q reference frame. The mathematical representation of the PMSM in the dq rotating coordinate system is given by the following equations under the following presumptions and using the dq coordinate transformation.

The equations for stator voltage in the d-q reference frame are:

$$V_q = R_s i_q + \omega_r \lambda_d + \rho \lambda_q \quad (3)$$

$$V_d = R_s i_d + \omega_r \lambda_q + \rho \lambda_d \quad (4)$$

The stator flux-linkage equations in the d-q reference frame are:

$$\lambda_q = L_q i_q \quad (5)$$

$$\lambda_d = L_d i_d + \lambda_f \quad (6)$$

Substitution of the resistance and current terms gives:

$$V_q = R_s i_q + \omega_r (L_d i_d + \lambda_f) + \rho L_q i_q \quad (7)$$

$$V_d = R_s i_d + \omega_r L_q i_q + \rho (L_d i_d + \lambda_f) \quad (8)$$

The mechanical rotor speed is:

$$\omega_m = \frac{2}{P} \omega_r \quad (9)$$

where R_s is stator resistance, L_q and L_q are the direct and quadrature axis inductances, λ_f is permanent-magnet flux linkage, and ω_r is electrical speed. Electromagnetic torque and mechanical dynamics are as follows:

$$T_e = \frac{3}{2}\left(\frac{P}{2}\right)(\lambda_d i_q - \lambda_q i_d) \quad (10)$$

$$T_e - T_L = J\frac{d\omega_m}{dt} + B\omega_m \quad (11)$$

Where P, T_e, T_L, J and B denote the number of poles, electromagnetic torque, external load, inertia and friction of the PMSM respectively.

Hysteresis current controller

Figure 2 illustrates the fixed based HCC for a phase. The HCC regulates the measured current, i_a within a prescribed band around the reference current, i_{ar}. The reference current is bounded by upper and lower thresholds. If the hysteresis half-band width is denoted by Δi, the upper current, i_{au} and lower boundaries, i_{al} are shown in equations 12 and 13 respectively. Three HCC are used for the three phase current controller.

$$i_{au} = i_{ar} + \Delta i \quad (12)$$

$$i_{al} = i_{ar} - \Delta i \quad (13)$$

$$HB = i_{au} - i_{al} = 2\Delta i \quad (14)$$

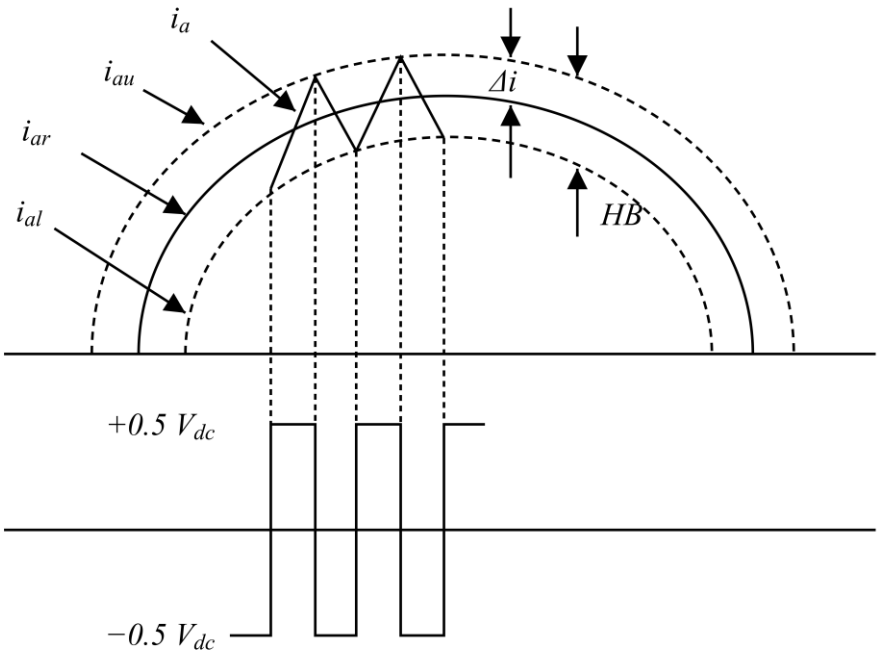

Figure 2: Operating principle of a fixed-band hysteresis current controller.

When the measured current reaches the upper threshold, a negative V_{DC} is produced; when it reaches the lower threshold, a positive V_{DC} is produced. This repeated switching confines the phase current to the selected band. A narrower band reduces tracking error but increases average switching frequency and switching loss. A wider band lowers switching frequency but increases current and torque ripple. The band should therefore be selected to balance tracking performance, torque ripple, and switching losses.

Voltage-source inverter

Three phase VSI serves as the power electronics interface to converts the DC bus voltage into three-phase AC variable voltages that drive the PMSM shown in Figure 3. The inverter stage takes the DC link voltage, V_{DC} and applies it to the motor terminals via a group of power switches that are controlled using the switching signals (Sa, Sb, Sc) generated by the HCC. The inverter contains three complementary switching legs connected to V_{DC}. Switches $S_a - S_{\bar{a}}$, $S_b - S_{\bar{b}}$ and $S_c - S_{\bar{c}}$ form the phase-A, phase-B, and phase-C legs. Antiparallel diodes provide current paths during commutation and regenerative operation.

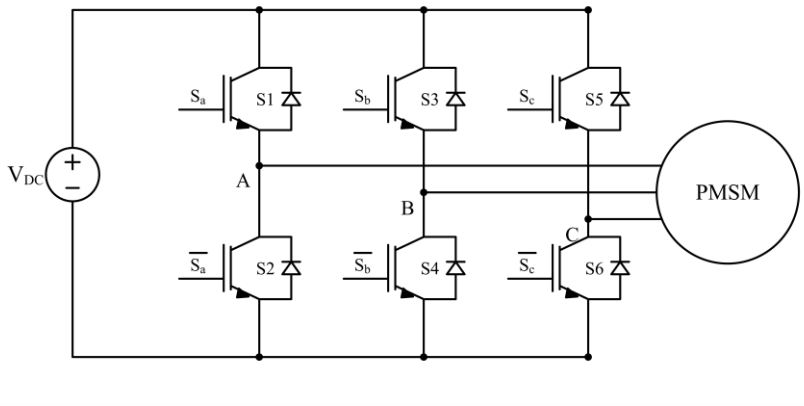

Figure 3: Three-phase two-level voltage-source inverter supplying the PMSM.

Speed controller design

This paper focused on the design and evaluation of the most popular and practical speed controller. The proportional integral (PI) are widely used in the high performance electrical drive system. The speed controller designed initially started with the conventional PI controller and followed by Anti Wind up Proportional Integral (AWPI). Finally, the paper propose a double AWPI (DAUPI) design and perform comparison analysis.

PI controller and output limiting

Based on the mathematical model of the PMSM, the speed of PI controller are calculated by using a second order system for a step input. The initial values for proportional (K_{ps}) and integral (K_{is}) gains of the three PI controllers are determined by comparing the general second order system with the close loop block diagram transfer function. Then the gains value are tuned to get the best value for the implementation. Figure 4 shows the PI speed controller block diagram where the speed error is processed by proportional and integral paths.

$$u = K_p \Delta\omega + \int K_i \Delta\omega \tag{13}$$

$$i_q^* = sat\,(u, +i_{qmax}, -i_{qmin}) \tag{14}$$

Their sum is limited to the permitted q-axis current range as shown in equation 14. The limiter protects the drive from excessive command current, but a limiter alone does not prevent integrator windup.

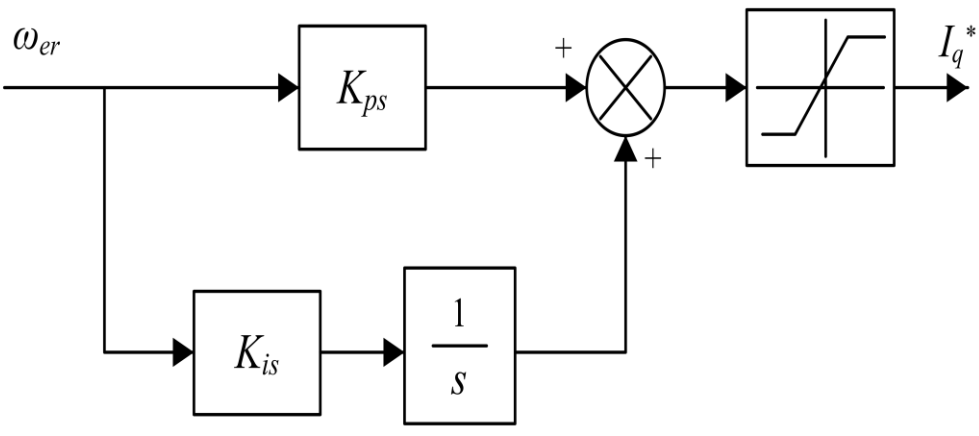

Figure 4: PI speed controller with output saturation.

Anti-windup PI controller and output limiting

The main objective of the snit wind up scheme is to avoid the over value or saturation value in integrator which causes high overshoot and long settling time. Large step change or large external load disturbance applied causes the PI controller saturate. This windup phenomenon results in inconsistency between the real plant input and the controller output. In order to overcome the wind up problem, the integral state is separately controlled [2], [12]. Thus, additional integral control in added to justified on the PI controller output is saturated or not based on the anti-windup structure in Figure 5. The integral term is only increased when certain conditions are satisfied, otherwise it is kept constant. Usually, the integration is stopped when the controller is saturated

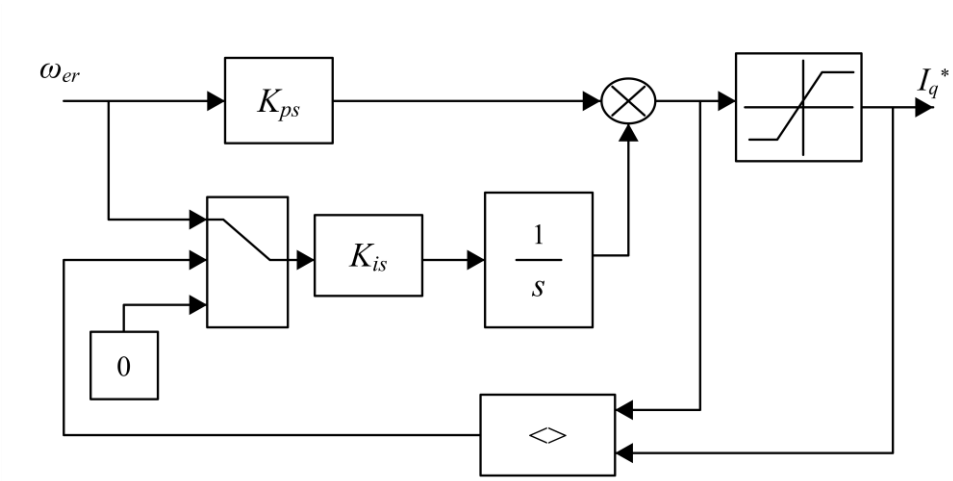

Figure 5: AWPI speed controller scheme.

Double-PI controller with anti-windup

Figure 6 shows proposed double PI controller with anti wind up (DAWPI) for the speed error. The primary path uses K_{ps} and K_{ps}, while the secondary path uses K_{ps2} and K_{ps2}. A comparator monitors saturation and governs the additional integral action. They aim is to improve the overall system performance such as overshoot, settling time, rise time and steady state error. The second PI design retain the simplicity, ease of implementation, and provide flexibility of the control and low cost controller used for the speed control system in AC motor drive system.

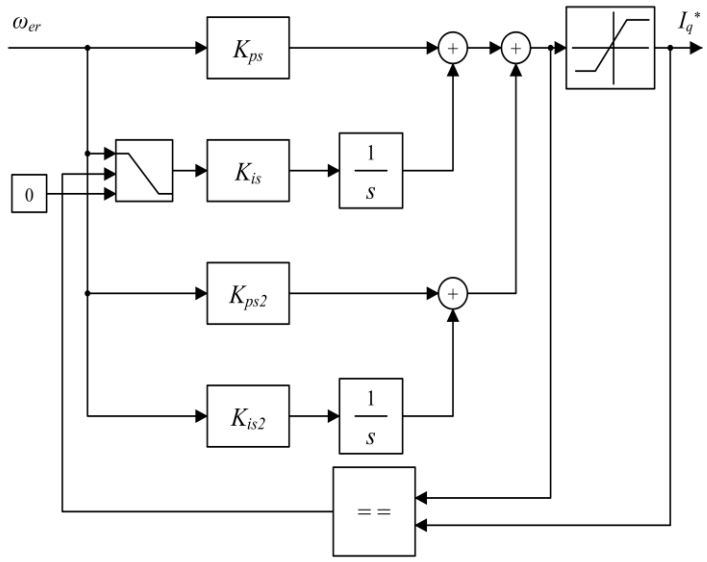

Figure 6: Double-PI speed controller with saturation-based anti-windup logic.

Simulation setup

The performance of PMSM will be evaluated based on the speed response produced by comparing between three type of speed controller which are PI, AWPI and DAWPI. The complete drive was implemented in MATLAB/Simulink form the electrical and mechanical PMSM model, a two-level VSI, coordinate transformations, hysteresis current controller and the speed control loop. The performance comparison between PI, AWPI and DAWPI controller is conducted under load and unloaded condition. Three phase PMSM motors parameter are shown in Table 1 below.

Table 1: PMSM motor parameters.

Motor Specifications	Value
Rated Voltage	120 V
Rated Frequency	50 Hz
Poles	4
Rated Speed	1500 rpm
Stator Resistance	0.5 Ω
direct-axis stator inductance	0.002 H
quadrature-axis stator inductance	0.002 H
Rotor Flux constant	0.0775 V/rads
Inertia	0.002kgm2
Viscous Friction	0.0001 Nm/(rad/s)

During the implementation the Kps and Kis value of the PI controller are tune to achieve appropriate value. This value are maintains for to the other two controller. The current limier is set at 10A. For the propose DAWPI configuration, the value set are as Kps2=0.2 and Kis2-0.7. The gains of the speed controller are shown in Table 2.

Table 2: Speed-controller gains used in the simulation.

Controller	Kps	Kis	Kps2	Kis2
PI	0.5	25	—	—
AWPI	0.5	25	—	—
DAWPI	0.5	25	0.2	0.7

RESULTS AND DISCUSSION

No-load speed performance at rated speed

Figure 7 shows the superimposes of the three controller responses at rated speed, 1500 rpm under no load condition. The motor accelerates from rest at t=1 s, reverses at t=3 s, and reverse to stand still operation at t=5 s. All controllers able to work well in for quadrant operations and reach the steady-state commands, while their transient deviations differ.

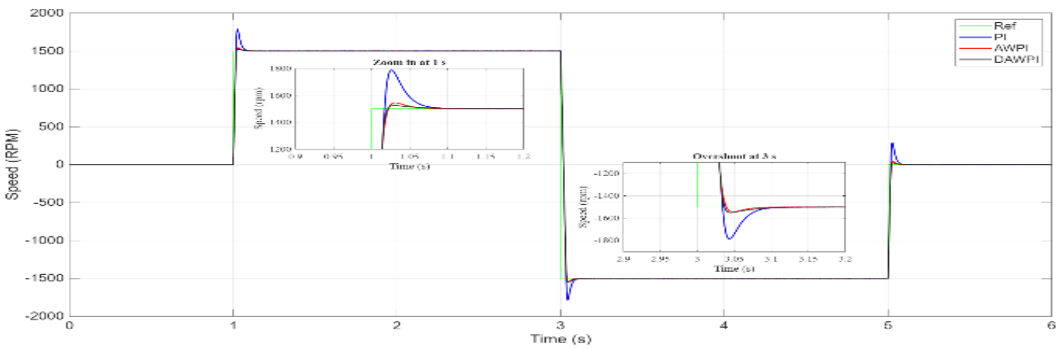

Figure 7: Rotor-speed responses of the PI, AWPI, and DAWPI controllers at rated speed.

Table 3 records the detail comparison of the overshoot (OS) and Rise time (Tr) of the controllers. At 1500 rpm, the measured peak speeds are 1769, 1546, and 1503 rpm for PI, PI-AW, and DAWPI. The corresponding overshoots are 17.93%, 3.07% and 1.24% respectively. DAWPI exhibits the smallest visible speed excursion and lower OS. For the Tr the PI controller reach fastest reference target with 1.017s follow b DAWPI and AWPI. DAWPI exhibits the smallest visible speed excursion and setting time. It is also observed that, all controller reach almost similar settling time (Ts).

Table 3: Start-up speed overshoot at a 1500 rpm reference.

Controller	Peak (rpm)	Deviation (rpm)	Overshoot (%)	Tr (s)
PI	1769	269	17.93	1.017
AWPI	1546	46	3.07	1.022
DAWPI	1524	24	1.60	1.021

Figure 8 shows the electromagnetic torque responses exhibit during transient pulses near 1, 3, and 5 s as the speed change demand from forward speed to reverse speed operation and back to the zero position. During the forward speed changed at 1s, the positive pulses provide positive torque to is limit value 10 Nm and decrease to zero torque when the speed reach 1500 rpm speed. A bit higher undershoot experience by PI controller. During the speed reversal, the negative pulse supports the speed reversal and returned to zero when the speed reach -1500 rpm. This is the normal torque speed character operate in four quadrant operation. PI exhibits more opposite-sign torque rebounds following the main pulses. These rebounds are less evident in the AWPI and DAWPI responses, indicating improved transient damping under the illustrated conditions. However, the overlapping traces do not permit a reliable quantitative distinction between AWPI and DAWPI. Following each transient, the torque returns to an oscillating band centered approximately around zero. Almost similar torque ripple are notified about 1.2Nm.

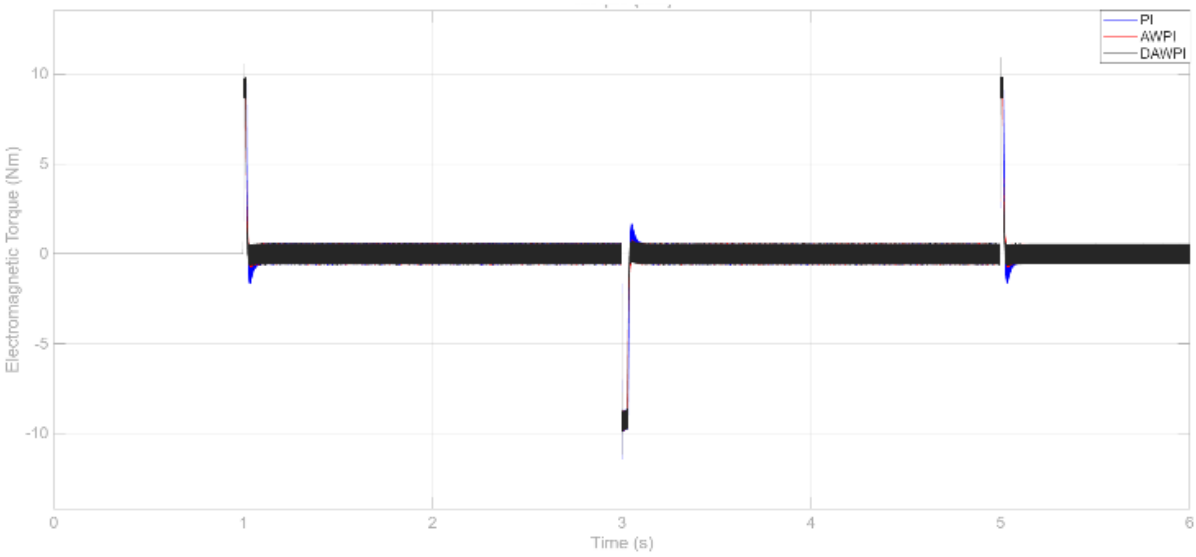

Figure 8: Electromagnetic torque responses during no-load forward and reverse operation at rated speed.

No-load speed performance at medium and low speeds

Further analysis is conducted to understand the speed performance operate below the rated speed. Figure 9 and Figure 9 compared the performance at medium 1000rpm and low 500rpm respectively based on the three controllers. The speed responses following the reference change to 1000 rpm at 1.0 s demonstrate differences in transient tracking performance. Conventional PI control exhibits a pronounced overshoot, reaching approximately 1222.3 rpm, whereas AWPI limits the peak to approximately 1045.6 rpm. DAWPI achieves the lowest peak, approximately 1020.3 rpm. These visually estimated values correspond to overshoots of approximately 22.23%, 4.56%, and 2.03%, respectively. Almost similar Tr are recorded for controller which is 1.011s.

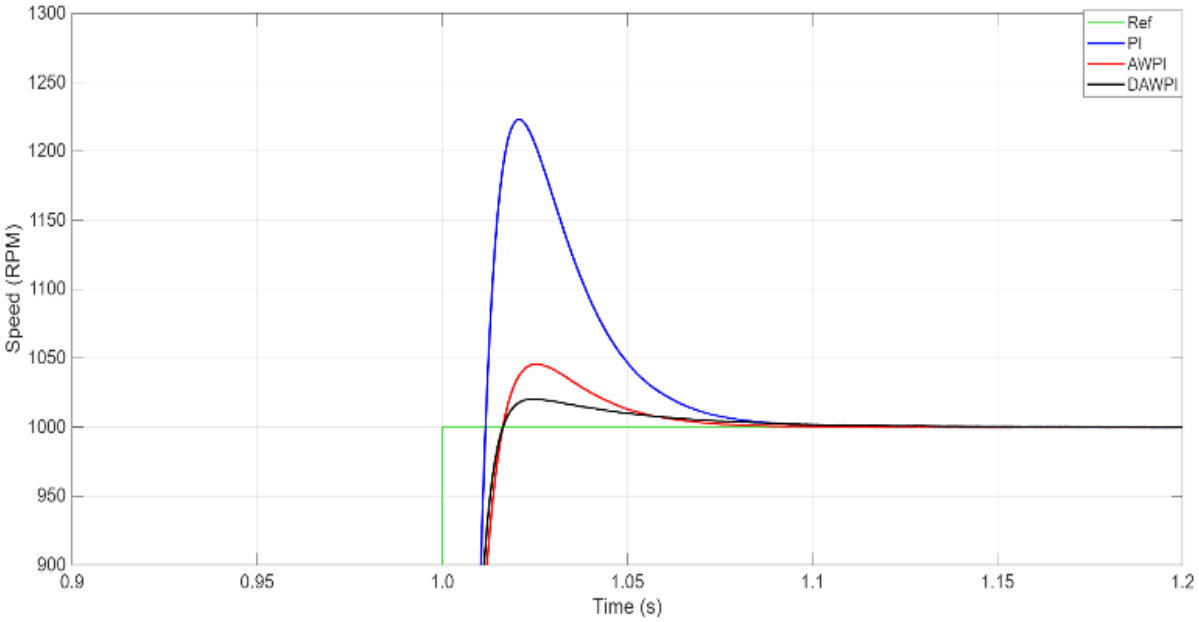

Figure 9: Enlarged start-up responses at a reference speed of 1000 rpm.

Figure 10 demonstrates the sped performance for the reference change demand from zero to 500 rpm at 1.0 s. The controllers exhibit different transient speed responses. PI reaches an estimated peak of 567.8 rpm, while AWPI and DAWPI reach approximately 556 rpm and 517.7 rpm, respectively. These peaks correspond to estimated overshoots of 13.6%, 11.2%, and 3.6%. Based on the above test, DAWPI provides the smallest overshoot among the three controllers under the medium and low speed operations. The DAWPI reduce the transient speed excursion and approach the reference more smoothly.

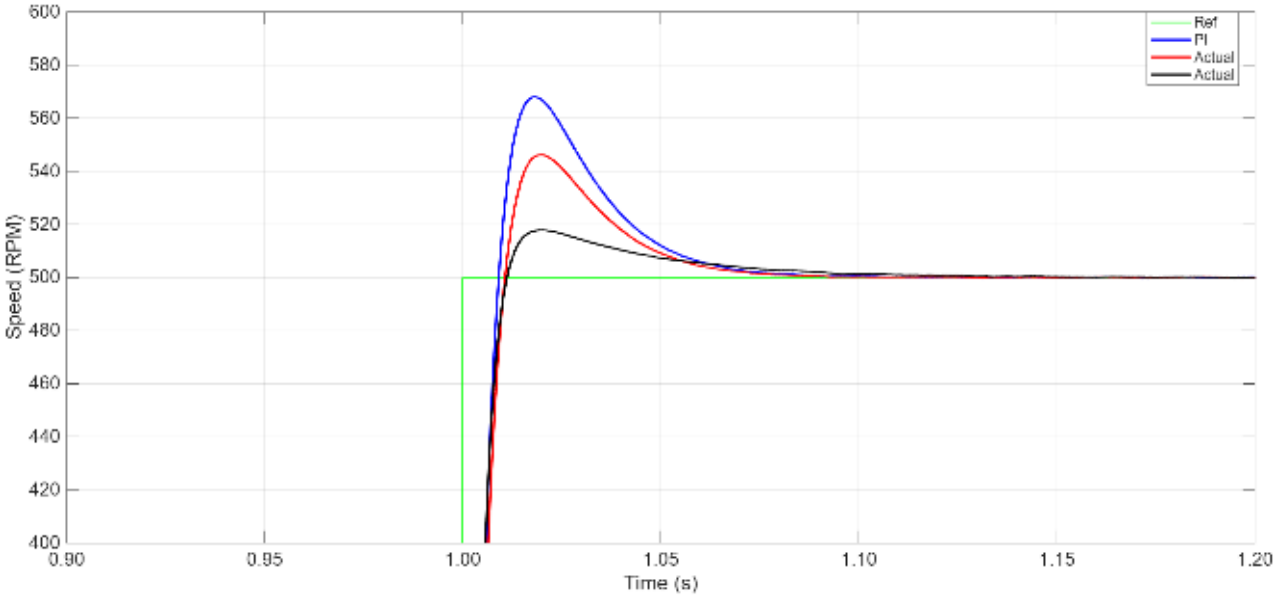

Figure 10: Enlarged start-up responses at a reference speed of 500 rpm.

Load test at rated speed and rated load

Further analysis is conducted to understand the speed performance operate at rated speed at 5 N·m load disturbance. The disturbance events are interpreted as load application and removal. Based on Figure 11, the load is applied at 1.5s and released the load at 2.5s. Based on the result, PI and AWPI exhibit overlapping responses, reaching approximately 1345 rpm after the disturbance near 1.5 s and 1381 rpm for DAWPI. The DAWPI experience 7.93% undershoot meanwhile the counterpart experience 10.3% undershoot. However, DAWPI faced longer recovery time which is 0.16s compare to 0.8% for PI and AWPI.

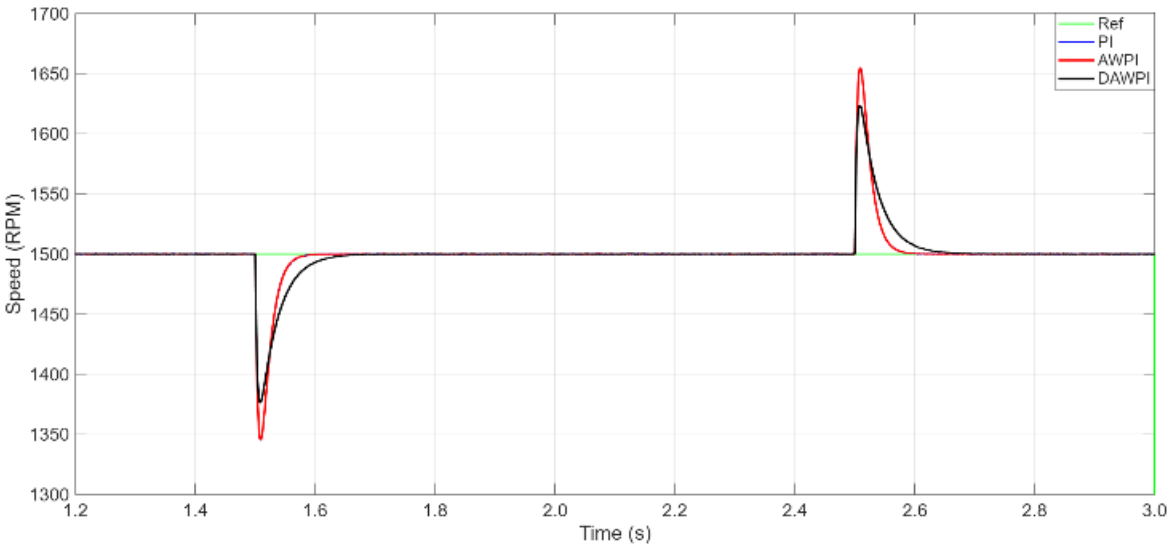

Figure 11: Speed response during application of a 5 N·m load at 1500 rpm.

During the unload condition at 2.5s, the deviation is therefore reduced from 151 rpm for PI/AWPI to 123 rpm for DAWPI, corresponding to an approximately 10.1% and 8.2% respectively. However, PI and AWPI recover towards the reference more rapidly, whereas DAWPI exhibits a longer decay. Thus, DAWPI provides better suppression of the peak speed excursion in this test, while PI and AWPI provide faster recovery. All responses approach the reference without sustained oscillation in the displayed interval. Exact recovery times and residual steady-state errors require numerical evaluation of the recorded signals.

Figure 12 shows the Ia phase-current responses of the PI, AWPI, and DAWPI. From starting the speed is increase from stand still to rated 1500 rpm. The external rated load is applied from 1.5 sec to 2.5 Sec before the command change the speed direction to reverse rated operation at 3 s. Finally the speed command change demand to operate at stand still at 5s. The current performance shows almost similar behavior to the speed demand changes where the current changed according during this times, The PI response appears to exhibit a larger negative excursion near 1 s nearly 20A follow by 16A for DAWPI and 14A for AWPI. During the load disturbance period, the current increase 12A peak for all the controllers. This is a appropriate phase current characteristic during the transient operation changed demand and load disturbances.

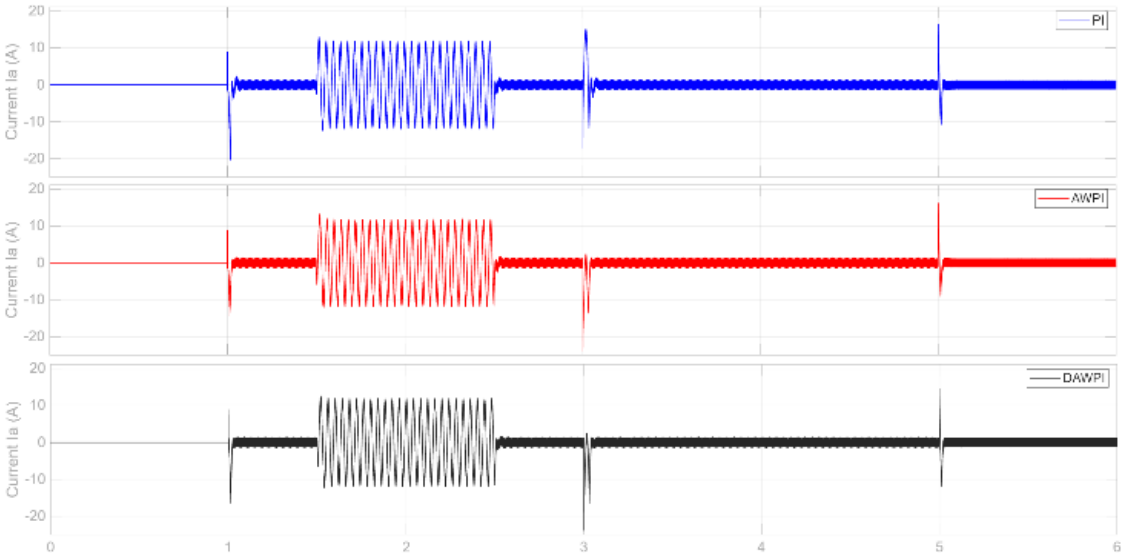

Figure 12: Phase-a current responses during transient operation and load disturbance.

CONCLUSION

This paper investigates the speed performance of field-oriented control (FOC) fed by HCC for PMSM drive. A MATLAB simulation model was developed to compare the conventional PI controller, AWPI, and proposed

DAWPI under various operating conditions for no load and loaded. The results support the benefit of proposed DAWPI controller by providing the lowest OS% and maintain the rise time response under low, medium dan rated speed operation significantly. The simple and flexible DAWPI controller configuration also demonstrate the ability to withstand load disturbance. The simulation results indicate that the DAWPI controller improving transient stator-current and comparable torque ripple current. Future work will focus on implementing the proposed practical and low cost controller in a physical PMSM drive. Experimental results can then be compared with the simulations to evaluate practical performance and identify the effects of switching delays, measurement noise, and hardware limitations.

ACKNOWLEDGEMENTS

The authors acknowledge the Faculty of Electrical Technology and Engineering, Universiti Teknikal Malaysia Melaka (UTeM), for guidance and resources supporting this work.

REFERENCES

1. Choi, H. H., Vu, N. T.-T., & Jung, J.-W. (2011). Digital implementation of an adaptive speed regulator for a PMSM. IEEE Transactions on Power Electronics, 26(1), 3–8. https://doi.org/10.1109/TPEL.2010.2055890
2. Choi, J.-W., & Lee, S.-C. (2009). Antiwindup strategy for PI-type speed controller. IEEE Transactions on Industrial Electronics, 56(6), 2039–2046. https://doi.org/10.1109/TIE.2009.2016514
3. Elmas, C., & Ustun, O. (2008). A hybrid controller for the speed control of a permanent magnet synchronous motor drive. Control Engineering Practice, 16(3), 260–270. https://doi.org/10.1016/j.conengprac.2007.04.016
4. Hazratgholi Zadeh Namin, S., Ghanbari, M., & Ebrahimi, R. (2025). A modified FOC strategy for 3-phase and 2-phase IMs using modified double PI controllers. The Journal of Engineering, 2025(1), Article e70077. https://doi.org/10.1049/tje2.70077
5. Jung, J.-W., Leu, V. Q., Do, T. D., Kim, E.-K., & Choi, H. H. (2015). Adaptive PID speed control design for permanent magnet synchronous motor drives. IEEE Transactions on Power Electronics, 30(2), 900–908. https://doi.org/10.1109/TPEL.2014.2311462
6. Khalid, M., Mohan, A., & Binojkumar, A. C. (2020). Performance analysis of vector controlled PMSM drive modulated with sinusoidal PWM and space vector PWM. In 2020 IEEE International Power and Renewable Energy Conference (pp. 1–6). IEEE. https://doi.org/10.1109/IPRECON49514.2020.9315210
7. Li, X.-L., Park, J.-G., & Shin, H.-B. (2011). Comparison and evaluation of anti-windup PI controllers. Journal of Power Electronics, 11(1), 45–50. https://doi.org/10.6113/JPE.2011.11.1.045
8. Ogbuka, C., Nwosu, C., & Agu, M. (2016). A fast hysteresis current-controlled permanent magnet synchronous motor drive based on field orientation. Journal of Electrical Engineering, 67(2), 69–77. https://doi.org/10.1515/jee-2016-0011
9. Ogbuka, C., Nwosu, C., & Agu, M. (2017). A high performance hysteresis current control of a permanent magnet synchronous motor drive. Turkish Journal of Electrical Engineering and Computer Sciences, 25(1), 1–14. https://doi.org/10.3906/elk-1505-160
10. Saidur, R., Mekhilef, S., Ali, M. B., Safari, A., & Mohammed, H. A. (2012). Applications of variable speed drive (VSD) in electrical motors energy savings. Renewable and Sustainable Energy Reviews, 16(1), 543–550. https://doi.org/10.1016/j.rser.2011.08.020
11. Santhakumar, C., Jayakumar, V., Chokkalingam, B., & Padmanaban, S. (2026). Hybrid hysteresis–FOC strategy with extended Clarke transformation for high-performance five-phase PMSM drives. IET Power Electronics, 19(1), Article e70229. https://doi.org/10.1049/pel2.70229
12. Talib, M. H. N., Ibrahim, Z., Abd. Rahim, N., & Abu Hasim, A. S. (2014). Comparison analysis of indirect FOC induction motor drive using PI, anti-windup and pre filter schemes. International Journal of Power Electronics and Drive Systems, 5(2), 219–229. https://doi.org/10.11591/ijpeds.v4i4.6250
13. Talib, M. H. N., Mat Isa, S. N., Hamidon, H. E., Ibrahim, Z., & Rasin, Z. (2016). Hysteresis current control of induction motor drives using dSPACE DSP controller. In 2016 IEEE International Conference on Power and Energy (PECon) (pp. 522–527). IEEE. https://doi.org/10.1109/PECON.2016.7951617

14. Wang, G., Zhang, G., & Xu, D. (2020). Position sensorless control techniques for permanent magnet synchronous machine drives. Springer. https://doi.org/10.1007/978-981-15-0050-3
15. Wang, H., & Leng, J. (2018). Summary on development of permanent magnet synchronous motor. In 2018 Chinese Control and Decision Conference (CCDC) (pp. 689–693). IEEE. https://doi.org/10.1109/CCDC.2018.8407219
16. Wang, X., Na, R., & Liu, N. (2009). Simulation of PMSM field-oriented control based on SVPWM. In 2009 IEEE Vehicle Power and Propulsion Conference (pp. 1465–1469). IEEE. https://doi.org/10.1109/VPPC.2009.5289523
17. Zellouma, D., Bekakra, Y., & Benbouhenni, H. (2023). Field-oriented control based on parallel proportional–integral controllers of induction motor drive. Energy Reports, 9, 4846–4860. https://doi.org/10.1016/j.egyr.2023.04.008